# Morphology and properties of novel copoly(isocyanurate–urea)s formed by reaction injection moulding

**Anthony J. Ryan*, John L. Stanford and Xiao Qiu Tao**
*Polymer Science and Technology Group, Manchester Materials Science Centre, University of Manchester and UMIST, Grosvenor Street, Manchester M1 7HS, UK*
*(Received 27 March 1992; revised 12 January 1993)*

Novel copoly(isocyanurate–urea)s have been produced by reaction injection moulding (RIM). The materials were formed from ~2:1 weight ratio of polyisocyanate to polyoxypropylene polyamine in the presence of an organic trimerization catalyst. In some cases an aromatic diamine chain extender was also used. The effects of the polyether polyamine functionality and the incorporation of aromatic diamine chain extenders on the morphology and properties of the copoly(isocyanurate–urea)s were studied using the SAXS, TEM, d.m.t.a. and tensile stress–strain techniques. The RIM materials were stiff plastics with room-temperature Young's moduli between 1.5 and 0.7 GPa, depending on the morphology. Development of morphology is a result of competition between polymerization kinetics, chemical gelation and (micro)phase separation. Materials with an isotropic, co-continuous morphology with a size-scale of ~100 Å had higher moduli than materials containing isolated glassy particles of ~1 μm in size. Correlations between morphology and dynamic mechanical-thermal and tensile stress–strain properties of a systematic series of copoly(isocyanurate–urea)s have been established.

**(Keywords: copoly(isocyanurate–urea)s; reaction injection moulding; morphology; SAXS; TEM)**

## INTRODUCTION

Isocyanurate-based polymers are of interest as matrix materials for structural composites formed by reaction injection moulding (SRIM), due to their good thermal and mechanical properties and because the reactant systems that are used to form such polymers allow controlled variations in processing parameters[1]. Current commercial SRIM systems such as SpectRIM MM373® (Dow Chemical) are based on polyether polyols and aromatic polyisocyanates. In these copoly(isocyanurate–urethane)s the polyol is used as a carrier for the trimerization catalyst required for isocyanurate formation, as shown in *Scheme 1*. The polyol provides control over mould-filling viscosity[2,3], gel conversion and gel time[4–6] during the SRIM process. In addition, the polyol is incorporated into the copolymer as a rubber microphase and affects final mechanical properties by acting as a toughening agent for the intrinsically brittle isocyanurate resin[7]. SRIM systems based on polyether polyamines and polyisocyanates to form copoly(isocyanurate–urea)s are not commercially available despite the advantages, in terms of improved thermal stability and mechanical properties, of using amine-functionalized (rather than hydroxyl-functionalized) polyethers to form RIM elastomers[1,8–10].

Copolyisocyanurate network-forming systems involve multiple competitive reactions and produce materials with complex morphologies. In these materials the chemical structure of the polymer, and the competition between polymerization reactions, microphase separation and vitrification, determine the morphology, which strongly influences the resulting properties of the materials. The work reported[2–7] to date has dealt solely with copoly(isocyanurate–urethane)s and has been restricted to studies of chemical (adiabatic) kinetics and mechanical properties, but without detailed reference to morphology. In contrast, the morphologies of the related block copolyurethanes have been studied extensively in attempts to interpret their thermal and mechanical properties. The techniques used to characterize morphology include small-angle X-ray scattering (SAXS), wide-angle X-ray diffraction (WAXD), transmission electron microscopy (TEM), scanning electron microscopy (SEM), and Fourier transform infra-red (*FT*i.r.) spectroscopy. Such studies have been the subject of a number of reviews[11–13].

This paper presents the results of studies on novel copoly(isocyanurate–urea)s[14] formed by RIM. The effects, of both the functionality of the polyether polyamine and the incorporation of aromatic diamine chain extenders, on the copoly(isocyanurate–urea) morphology are characterized by SAXS and TEM. Correlations between morphology and dynamic mechanical-thermal and tensile stress–strain properties of a systematic series of copoly(isocyanurate–urea)s are established.

## EXPERIMENTAL

### *Reactants*

The materials in this study were formed using three components, i.e. a polyisocyanate, a polyether polyamine and an organic catalyst. In some cases an aromatic

* To whom correspondence should be addressed

0032-3861/93/194020-12

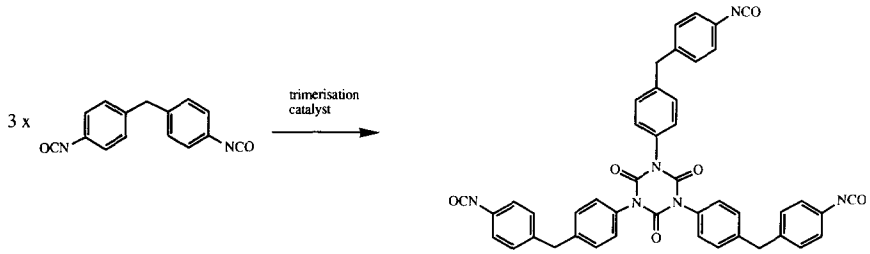


**Scheme 1** Formation of the simplest triisocyanurate structure from MDI

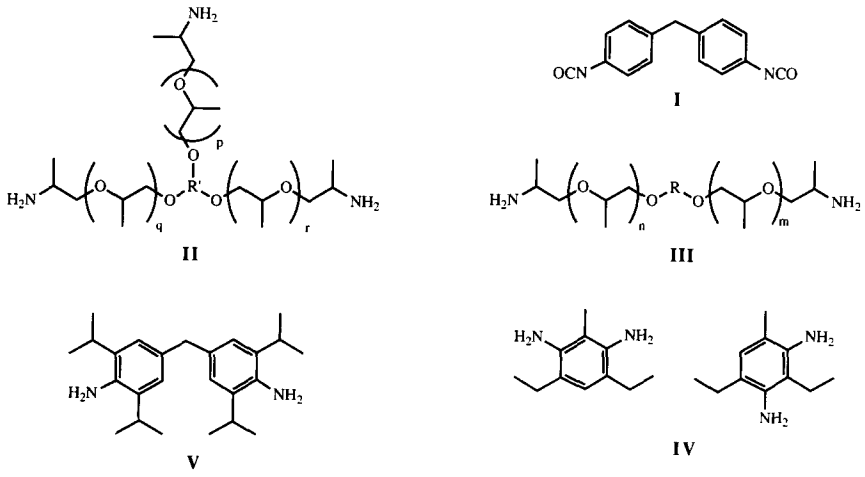


**Scheme 2** Idealized monomer structures

diamine chain extender was also used. The chemical structures of the various reactants used are shown in *Scheme 2*.

The polyisocyanate, Isonate M143 (Dow Chemical), is a uretonimine-modified version of 4,4′-diphenylmethane diisocyanate (MDI) (I), and is a straw-coloured, low-viscosity liquid (0.02 Pa s at 25°C) with an equivalent weight of $143 \pm 2\,g\,mol^{-1}$ (by isocyanate titration)[15]. Jeffamine T5000 (Texaco Chemical Company) is a polyoxypropylene triamine (II) with a nominal molar mass of $5000\,g\,mol^{-1}$ and an equivalent weight of $1900\,g\,mol^{-1}$ ($-NH_2$), and Jeffamine D2000 (Texaco Chemical Company) is a polyoxypropylene diamine (III) with a nominal molar mass of $2000\,g\,mol^{-1}$ and an equivalent weight of $980\,g\,mol^{-1}$ ($-NH_2$). The trimerization catalyst, DABCO–TMR® (Air Products), is a quaternary ammonium carboxylate, *N*-hydroxypropyl-trimethylammonium-2-ethylhexanoate. The aromatic diamine chain extender used was either 3,5-diethyltoluene diamine (DETDA) (IV) (as an 80:20 mixture of the 2,4- and 2,6-isomers), or 4,4′ methylenebis(2,6-diisopropylaniline) (MDIPA) (V). The chain extenders (Lonza AG) were thoroughly characterized by combustion analysis and n.m.r. spectroscopy prior to use. All reactants were used as received without further purification.

*Reaction injection moulding*

Poly(isocyanurate–urea)s were moulded as rectangular plaques ($150 \times 400 \times 3$ mm) using in-house RIM equipment that has been described in detail elsewhere[16]. The overall stoichiometric ratios, defined as the ratio of isocyanate to amine groups, and the amounts of catalyst used are given in *Table 1*. Each copolymer is designated by a material code comprising three terms, namely polyamine type/hard-segment type/catalyst level. The polyamine types are d2 = D2000 and t5 = T5000; the hard segment types are m = MDI-based isocyanurate, 20d = DETDA and MDI-based isocyanurate, and 20m = MDIPA and MDI-based isocyanurate; the catalyst level refers to the parts by weight of catalyst to 203.2 parts of M143. A constant mass ratio of 2.032:1 was used throughout. A machine throughput of $\sim 60\,g\,s^{-1}$ was used for the polyamine reactant stream, while the corresponding throughput of the polyisocyanate reactant stream was $\sim 120\,g\,s^{-1}$. Initial reactant and mould temperatures of 36 and 90°C, respectively, were used throughout, and typical gel times were of the order of 4 s with mould filling occurring in 1.4 s. Plaques were removed from the mould after a period of at least 5 min. To achieve good mixing in an impingement mixing device, nozzle Reynolds numbers must exceed a critical value[1]. Thus the Reynolds number for the polyamine reactant stream was held constant at $\sim 500$, which is greater than the critical value of $\sim 300$ generally quoted for polyurea formulations[1]; the Reynolds number for the polyisocyanate reactant stream was $> 1500$. Mixing was therefore good and the materials showed no visible striations or gel lines.

*Dynamic mechanical thermal analysis*

D.m.t.a. data were obtained on a Polymer Laboratories machine at a frequency of 1 Hz in the temperature range $-100$ to 300°C at a heating rate of $5°C\,min^{-1}$. A double cantilever bending geometry was used for beam samples ($3 \times 10 \times 45$ mm) to obtain dynamic flexural moduli and mechanical damping as functions of the temperature.

*Tensile stress–strain*

Data were obtained on an Instron 1122 Universal Testing Machine at $20 \pm 3$°C. Dumb-bell specimens

**Table 1** Formulations and stoichiometric ratios (*r*) used to form copoly(urea–isocyanurate)s

| Copolymer[a] | Components (parts by weight) | | | | | | |
|---|---|---|---|---|---|---|---|
| | M143 | D2000 | T5000 | DEDTA | MDIPA | TMR | *r*[b] |
| d2/m/1.6 | 203.2 | 100.0 | – | – | – | 1.6 | 13.9 |
| d2/m/0.6 | 203.2 | 100.0 | – | – | – | 0.6 | 13.9 |
| t5/m/1.6 | 203.2 | – | 100.0 | – | – | 1.6 | 27.0 |
| d2/20d/1.6 | 225.0 | 100.0 | – | 11.0 | – | 1.8 | 7.0 |
| d2/20m/1.6 | 236.2 | 100.0 | – | – | 16.2 | 1.9 | 8.6 |
| t5/20d/1.6 | 224.2 | – | 100.0 | 10.3 | – | 1.8 | 9.3 |

[a] Copolymers are designated by material codes comprising three terms, namely polyamine type/hard-segment type/catalyst level: polyamine types are d2 = D2000, and t5 = T5000; hard-segment types are m = MDI-based isocyanurate, 20d = DETDA and MDI-based isocyanurate, and 20m = MDIPA and MDI-based isocyanurate; catalyst level refers to the parts by weight of catalyst to 203.2 parts of M143
[b] Ratio of NCO groups to total $NH_2$ groups

(ASTM D638m), having an overall length of 150 mm, a neck length of 60 mm, a width of 12.5 mm and a thickness of ~3 mm were used. The gauge length was 75 mm and the extension rate 10 mm $min^{-1}$. Strains were recorded to within ±0.05% using a 0–10% strain-gauge extensometer clamped directly onto the central portion of a dumb-bell specimen. The tensile properties reported are the mean values of at least five tests.

*Transmission electron microscopy*

Samples were microtomed using a Reichert–Jung Ultracut E with a freshly prepared, wet glass knife at room temperature. The knife trough was filled with distilled water and thin sections were floated onto 500-mesh copper TEM grids. Optical reflection indicated, by the gold colour, that sections were <40 nm thick. A Phillips 301 Transmission Electron Microscope, operated at 100 kV, with magnifications between 7500 and 28 000, was used with Grade IV Ilford film. Microtomed thin sections were observed directly without any support film. To minimize electron beam damage of the samples and also to avoid radiation artifacts, special precautions were taken by focusing on one area and translating to an adjacent area for recording. Contrast was enhanced by underfocus of the objective lens.

*Small-angle X-ray scattering*

SAXS measurements were made on beamline 8.2 on the Synchrotron Radiation Source (SRS) at the SERC Daresbury Laboratory, Warrington, UK; the camera geometry and electronics have been described in detail elsewhere[17]. Scattering from an oriented specimen of wet collagen (rat-tail tendon) was used to calibrate the sample-to-detector distance (~3.5 m). The specimens for SAXS were prepared by cutting strips 3 × 10 × 50 mm from RIM plaques. Scattering patterns were taken by fixing the ends of the specimens onto the entrance window of the camera's vacuum chamber so that the X-rays could pass uninterrupted and data were collected for periods of one minute per specimen. Parallel-plate ionization detectors, placed before and after the sample record the incident and transmitted intensities, thus enabling differences in the specimen's attenuation factors (a function of transmission and thickness) to be monitored. The experimental data were corrected for background scattering (subtraction of the scattering from the empty camera), attenuation factor and the positional alinearity of the detector. The reproducibilities of the spatial resolution and integrated intensities were ±1% and ±2%, respectively.

*SAXS data analysis*

A peak or a shoulder in $I(\mathbf{q})$ gives a general indication of the presence of a periodic structure in the system. The most common practice for determining the periodicity is to use Bragg's law in the calculation of a domain spacing, *d*, from the location of the peak maximum, $\mathbf{q}_{max}$, in an intensity *versus* scattering vector plot:

$$d = \lambda/2 \sin\theta_{max} = 2\pi/\mathbf{q}_{max}$$

The shoulder in the bare intensity data shown in *Figure 1* is weak, making unambiguous determination of $\mathbf{q}_{max}$ difficult, if not impossible. For the copolymers in the present study, more precise information regarding microstructural periodicity is obtained if the morphology is assumed to be globally isotropic but locally lamellar[18]. (The choice of a lamellar morphology for data analysis is based on the stoichiometry of the system; the volume fraction of the electron-dense phase is ~0.57.) The data can then be analysed to give a one-dimensional Bragg spacing (*1-d*), by applying the Lorentz correction, $\mathbf{q}^2$, to the observed scattered intensity $I(\mathbf{q})$. *Figure 1* shows plots of $I(\mathbf{q})$ and $I(\mathbf{q})\mathbf{q}^2$ *versus* $\mathbf{q}$ for the copolymer d2/m/0.6. The upturn of $I(\mathbf{q})\mathbf{q}^2$ at high $\mathbf{q}$ in *Figure 1* indicates a positive deviation[18] from Porod's law[19], caused by either a strong thermal fluctuation background or isolated segmental mixing. For materials with sharp phase boundaries, Porod's law[19] predicts a fall off of $\mathbf{q}^{-4}$ in scattered intensity at large angles:

$$\lim_{\mathbf{q}\to\infty} I(\mathbf{q}) = (K_p/\mathbf{q}^4) + I_b$$

The quantity $I_b$ arises from density fluctuations and $K_p$ is the Porod constant. It is important to note the strong positive deviation in the Porod plot ($I(\mathbf{q})\mathbf{q}^4$ *versus* $\mathbf{q}^4$), which is illustrated as an inset to *Figure 1* for the d2/m/0.6 material. Positive deviations from Porod's law are caused by thermal density fluctuations and/or isolated mixing of one type of segment in the other[12]. A regression analysis of the linear part of the curve gives values of $K_p = 15.4$ and $I_b = 2.95 \times 10^4$. $I_b$ must be subtracted from the raw intensity data before both *1-d* and the invariant are calculated.

The filled symbols in *Figure 1* are values of $I'\mathbf{q}^2[=(I(\mathbf{q})-I_b)\mathbf{q}^2]$ *versus* $\mathbf{q}$; the artificial upturn of $I(\mathbf{q})\mathbf{q}^2$ at high $\mathbf{q}$ has been corrected. For the calculation of the

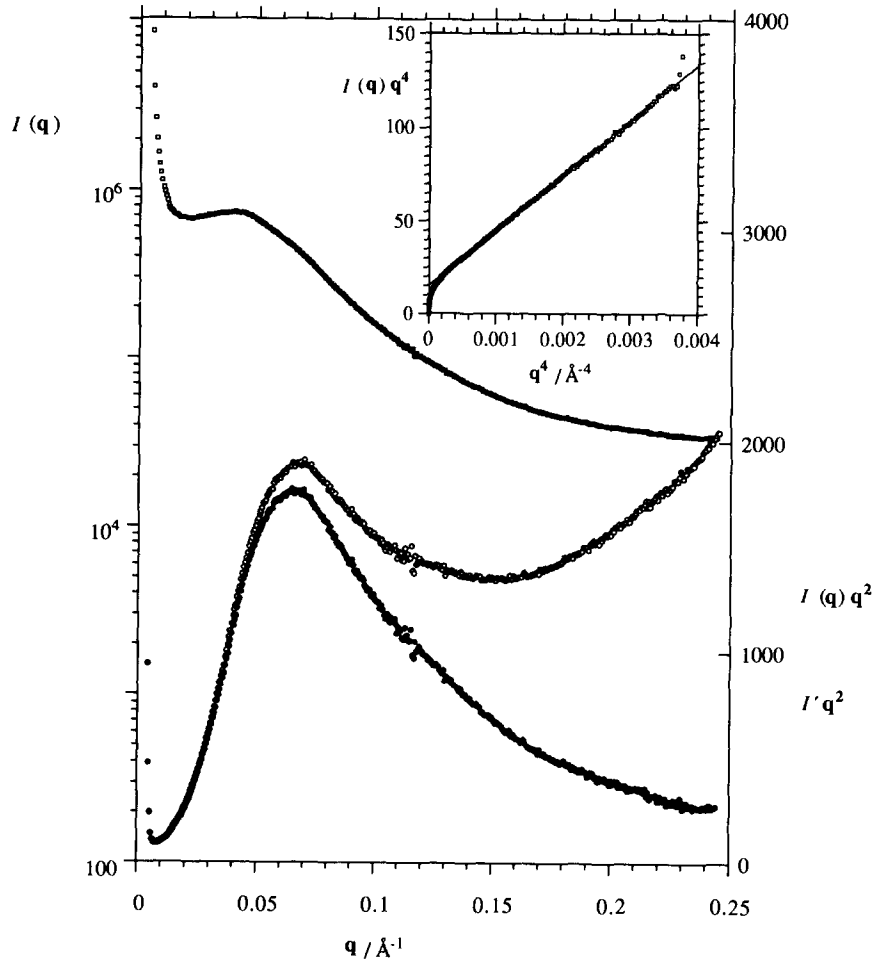


**Figure 1** Scattering curves for the d2/m/0.6 copolymer, showing the three stages of data analysis: the upper curve (□) is the bare intensity, $I(\mathbf{q})$, *versus* $\mathbf{q}$; the middle curve (○) is the Lorentz-corrected intensity, $I(\mathbf{q})\mathbf{q}^2$, *versus* $\mathbf{q}$ and; the lower curve (●) of $I'\mathbf{q}^2$ *versus* $\mathbf{q}$ is the Lorentz-correction of the bare intensity with the thermal background subtracted. The inset is a Porod plot of $I(\mathbf{q})\mathbf{q}^4$ *versus* $\mathbf{q}^4$ for this material: the symbols (□) are data points and the solid line is a regression analysis of the linear part of the curve, giving values of $K_p = 15.4$ and $I_b = 2.95 \times 10^4$

Bragg spacing, the maximum in $I'\mathbf{q}^2$ *versus* $\mathbf{q}$ is taken as $\mathbf{q}^*$, so that $l\text{-}d = 2\pi/\mathbf{q}^*$. The peak value from $I(\mathbf{q})$ *versus* $\mathbf{q}$ gives a $d$ spacing of $\sim 150$ Å whereas the peak value from $I'\mathbf{q}^2$ *versus* $\mathbf{q}$ gives a $l$-$d$ spacing of 95 Å. The fully corrected value of this spacing ($l$-$d$) will be used in the discussion that follows.

The invariant ($Q$) is a linear function of the electron density difference, $\langle\eta^2\rangle$, between the polyether and crosslinked isocyanurate rich phases and is obtained from the integral:

$$\langle\eta^2\rangle = \frac{Q}{2\pi i_e} = \frac{1}{2\pi i_e}\int_0^\infty (I(\mathbf{q}) - I_b)\mathbf{q}^2\, d\mathbf{q} = \frac{1}{2\pi i_e}\int_0^\infty I'\mathbf{q}^2\, d\mathbf{q}$$

where $i_e$ is the Thompson scattering factor. The invariant $Q$ is independent of the size or shape of the structural heterogeneities. The absolute value of the invariant requires absolute intensity measurements, thermal background subtraction, and extrapolation to $\mathbf{q} = 0$ and $\infty$ and is computationally difficult to achieve. The major contribution to the experimental invariant can be used to characterize structure development, as well as the degree of microphase separation, and is readily assessed by a Simpson's rule integration of the ($I(\mathbf{q})\mathbf{q}^2$ *versus* $\mathbf{q}$) curve between experimental limits[17]. A relative invariant, $Q'$, has been calculated by summation of the area under the ($I'\mathbf{q}^2$ *versus* $\mathbf{q}$) curve between the first reliable data point, $\mathbf{q} = 0.01$ Å$^{-1}$, and the region in which $I'\mathbf{q}^2$ becomes constant, i.e. at $\mathbf{q} = 0.25$ Å$^{-1}$. Due to the relative nature of the intensity measurement the value of $Q'$ is also only relative, with arbitrary units.

## RESULTS AND DISCUSSION

The RIM materials were stiff plastics with room-temperature Young's moduli between 1.5 and 0.7 GPa. The macro-network structure of these copoly(isocyanurate–urea)s is not easy to visualize but the values of the moduli suggest that there is a continuous glassy phase[8]. The simplest materials are formed from two of the components, namely the polyisocyanate and either the polyether diamine or the polyether triamine, and these materials comprise 33% by weight (43% by volume) of polyether and 67% by weight (57% by volume) of highly crosslinked polyisocyanurate. Assuming that the impingement mixing process produces a homogeneous mixture on the molecular level, the stages of polymerization can then be described. In the initial stages of copolymerization, –NCO-tipped, polyether–urea oligomers are formed by the nearly instantaneous[20] reaction between aliphatic –$NH_2$ groups and the large stoichiometric excess of isocyanate groups. The remaining isocyanate

groups then undergo trimerization reactions, at a rate determined by the catalyst content and temperature, to form a highly crosslinked material. Good connectivity between the polyisocyanurate and polyether microphases is ensured by the initial formation of the urea bonds. During the polymerization process there is a large increase in average molecular weight and a change in chemical structure causing both rapid microphase separation and polyisocyanurate vitrification, which quench the system to produce an incompletely reacted material with a non-equilibrium morphology.

There is strong experimental evidence to support the existence of a microphase-separated morphology, even if the morphology is difficult to define in terms of either lamella, interconnected rods or isolated spheres. The use of TEM micrographs to determine morphology in block copolymers can lead to conflicting conclusions. For example, the micrographs shown in *Figure 2* for the d2/m/0.6 copolymer show a two-phase morphology, with a dominant wavelength of $\sim 100$ Å, which appears similar to Cahn and Hilliard's[21] computer simulation of a random co-continuous spinodal structure: this morphology is also reminiscent of that observed by TEM for a segmented copolyurethane, described by Thomas and co-workers[22] as 'a random-platelet'. However, previous studies[23] of RIM copolyureas indicate that the dominant mechanism of morphology formation is by spinodal decomposition, which is initiated at low conversions of the isocyanate groups. The assumption of a random lamella morphology and use of the Lorentz correction is, to some extent, suggested by the TEM micrographs; however, the two-dimensional projection of a random three-dimensional structure is notoriously difficult to interpret. The diffraction patterns, and the Porod plot shown in *Figure 1*, correspond to the structure in *Figure 2a*, and suggest a well ordered system with a size-scale of $\sim 100$ Å, with diffuse phase boundaries; the SAXS data are in good agreement with the TEM results. The positive deviation in the Porod plot comes from either isolated glassy segments or a strong thermal fluctuation in electron density: the lack of higher-order peaks in the SAXS patterns is typical of segmented block copolymers which are microphase-separated, but have sigmoidal rather than square interphase profiles and no long-range order[17]. The d.m.t.a. curves in *Figure 3* confirm the microphase-separated nature of this material. The polyether glass transition is observed as a peak in $\tan\delta$ and a drop in modulus at $\sim -50$°C. The isocyanurate glass transition is also observed as a peak in $\tan\delta$ and a drop in modulus (followed by a rubbery plateau) at higher temperatures ($>150$°C). The effects of processing and chemistry on the morphology and properties of the novel copoly(isocyanurate–urea)s are dealt with in more detail in the specific sections that follow.

*Effects of thermal treatment*

Simple materials with a relatively low catalyst content (i.e. d2/m/0.6) have a low rate of trimerization and have been subjected to a series of heat treatments. These materials have been shown to have the least complete reaction on demoulding, and are therefore the most susceptible to changes caused by heat treatment (annealing). The TEM micrographs shown in *Figure 2* are for unstained specimens which were (a) as-moulded, (b) annealed at 150°C for 1 h, and (c) annealed at 180°C for 1 h. The as-moulded material has a poorly defined structure. Image definition is due entirely to density differences between the microphases and is sharpened considerably by annealing at 150 and 180°C. The characteristic length in the micrographs is estimated to be $\sim 100$ Å and this does not change on annealing, and the dominant feature of the series of images (*Figures 2a–c*) is the increase in phase contrast with the annealing temperature. The Lorentz-corrected scattering curves, presented in *Figure 4*, are essential for calculation of the relative invariant, $Q'$, and illustrate the improvement in electron-density difference (phase purity) on annealing. The $Q'$ values given in *Table 2* show a 40% increase on annealing. The value of $Q'$ is independent of the size of the scattering centres and is a function only of the electron-density difference between the highly crosslinked glass and the rubbery polyether. Changes in $Q'$ correspond to changes in the degree of microphase separation and are in qualitative agreement with the contrast in the TEM micrographs. The (*1-d*) spacings that are obtained are

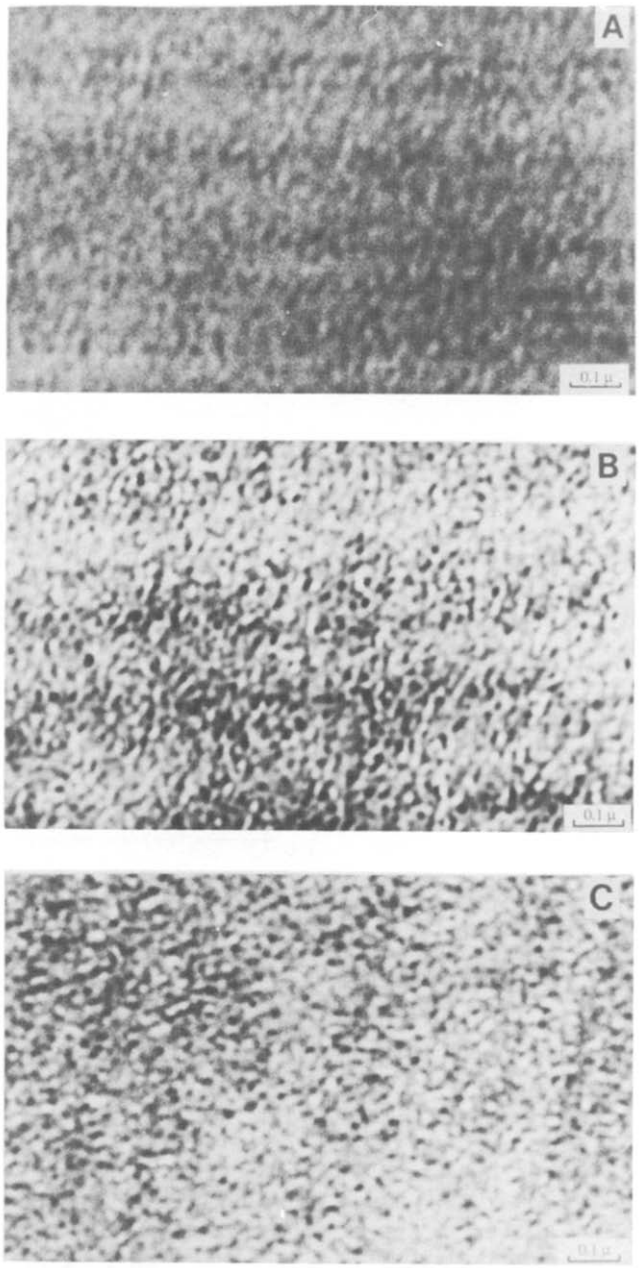


**Figure 2** TEM micrographs of the d2/m/0.6 copolymer: (A) as-moulded; (B) annealed 1 h at 150°C; and (C) annealed 1 h at 180°C

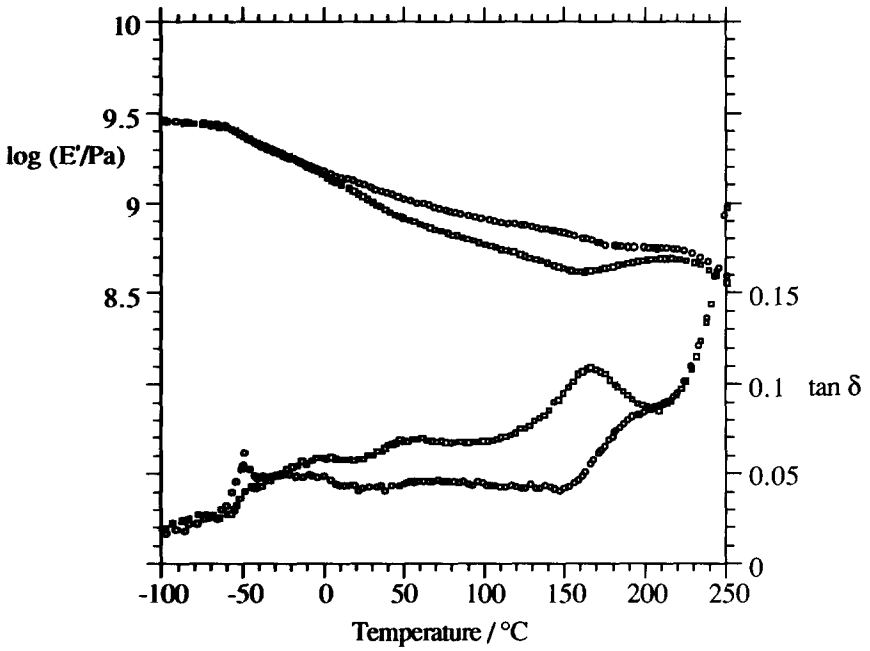


**Figure 3** D.m.t.a. curves of the d2/m/0.6 copolymer: (□) as-moulded and; (○) annealed 1 h at 150°C

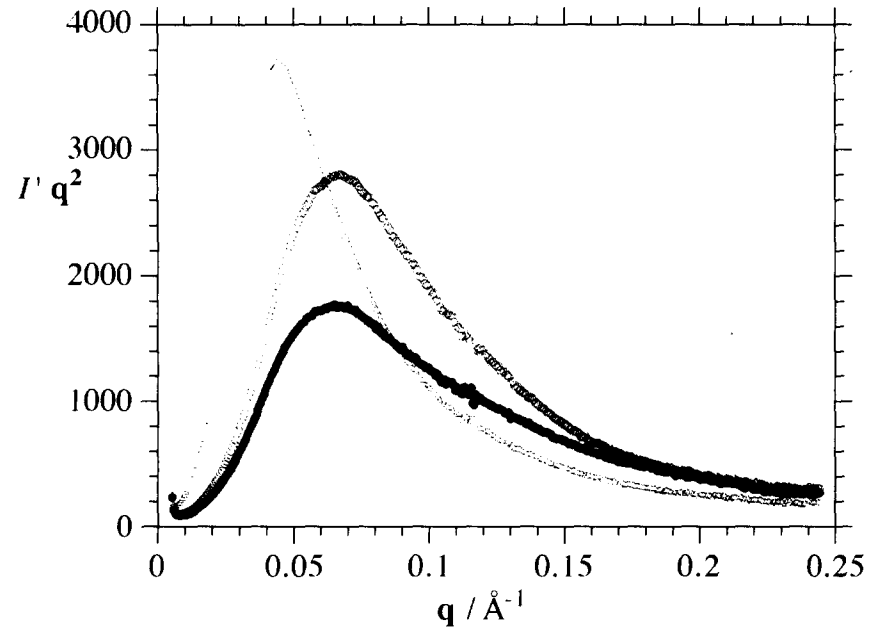


**Figure 4** Lorentz-corrected SAXS patterns for the d2/m/0.6 copolymer: (●) as-moulded; (○) annealed 1 h at 150°C; and (△) annealed 1 h at 180°C

**Table 2** Composition, morphology and tensile properties of RIM copoly(isocyanurate–urea)s

| Copolymer[a] | $\phi_{pe}$[b] | *l-d* (Å) | *Q'* | *L* (Å) | *E* (GPa) | $\sigma_u$ (MPa) | $\varepsilon_u$ (%) |
|---|---|---|---|---|---|---|---|
| d2/m/1.6 | 0.43 | 112 | 214 | 110 | 1.38±0.07 | 37±2.7 | 3.8±1.5 |
| d2/20d/1.6 | 0.38 | 74 | 180 | 70 | 1.53±0.12 | 52±1.9 | 8.0±1.5 |
| d2/20m/1.6 | 0.37 | 116 | 188 | 110 | 1.27±0.06 | 38±2.6 | 5.1±0.4 |
| t5/m/1.6 | 0.43 | 153 | 198 | 150 | 0.72±0.06 | 30±6.4 | 11.6±4.4 |
| t5/20d/1.6 | 0.39 | 98 | 187 | 100 | 0.80±0.04 | 42±4.8 | 15.3±3.6 |
| d2/m/0.6/n | 0.43 | 95 | 180 | 100 | 1.26±0.12 | 38±2.2 | 10.0±1.6 |
| d2/m/0.6/150 | 0.43 | 95 | 257 | 100 | 1.45±0.06 | 52±0.6 | 8.7±0.6 |
| d2/m/0.6/180 | 0.43 | 150 | 247 | 100 | 1.46±0.10 | 44±3.0 | 6.2±0.8 |

[a] n refers to the as-moulded material; 150 and 180 refer to the materials annealed at 150°C and 180°C for 1 h, respectively
[b] Volume fraction of polyether

95, 95 and 150 Å, respectively, for the as-moulded, 150°C- and 180°C-annealed materials. The $(l-d)$ spacing for the highest-temperature material is much larger than the value obtained for the as-moulded and 150°C-annealed materials, and could be due to Ostwald ripening[24] on annealing lightly crosslinked structures. The discrepancy between length scales estimated from TEM and $(l-d)$ values, calculated precisely from SAXS measurements, is insignificant and is more than compensated for by the correlations between techniques in terms of microphase contrast.

The structural changes which occur on annealing the d2/m materials are readily explained by the differences in the d.m.t.a. curves of *Figure 3* and by the tensile stress–strain data presented in *Table 2*. At low temperatures ($< -60$°C) both as-moulded and annealed materials have moduli ($\sim 3$ GPa) and low damping which are typical of a glassy polymer. As the temperature exceeds $-50$°C, the modulus begins to fall and $\tan\delta$ increases. The thermal sensitivity of the modulus and damping of the as-moulded and annealed materials is quite different. The annealed material has a sharp peak in $\tan\delta$, associated with the soft segment glass transition temperature at $\sim -45$°C, whereas $\tan\delta$ rises gradually with temperature for the as-moulded material, clearly indicating that the polyether-rich microphase is much purer in the annealed material. For both materials, the moduli decrease at the same rate up to 0°C, while above this temperature, the as-moulded material has much lower moduli and higher damping than the annealed material, due to its lower degree of crosslinking and microphase separation. The as-moulded material has a weak peak in $\tan\delta$ and a corresponding change in slope of $E'$ at $\sim 50$°C and this feature, often observed in other RIM copolyureas[8,9], is normally ascribed to the breakdown of hydrogen bonding between the ether oxygens and the urea groups. Both of the modulus–temperature curves have inflections at $\sim 160$°C. For the as-moulded material, $E'$ gradually increases and there is a corresponding peak in $\tan\delta$, and this behaviour is associated with two opposing processes, namely a glass–rubber relaxation and a preceding crosslinking reaction. Between 160 and 200°C, the annealed material shows an initial decrease in $E'$, followed by a modulus plateau with the corresponding $\tan\delta$ values rising to a shoulder, and this behaviour is associated with a relaxation in the isocyanurate-rich microphase. Above 220°C, $E'$ begins to decrease and $\tan\delta$ increases rapidly for both materials as thermal-oxidative degradation occurs. Generally, the d.m.t.a. data show the as-moulded material to be incompletely reacted and also poorly micro-phase separated; annealing increases the modulus (by forcing the reaction toward completion, thereby increasing crosslink density) and reduces the damping (by improving the level of microphase separation). Tensile stress–strain data confirm one of the effects of annealing, i.e. an increase in crosslink density, which explains an increased Young's modulus and reduced ultimate elongation with annealing. The interpretation of the damping behaviour, as regards improvement of phase purity with annealing, is in good agreement with the SAXS and TEM results.

*Effects of hard segment structure*

The addition of a hindered aromatic diamine (typically used as chain extenders in RIM polyureas)[1,8–10,16,20,23] was investigated. The addition of a chain extender was observed to significantly increase the mould-filling viscosity of these systems. The overall polymerization still effectively comprises a two-stage reaction process involving instantaneous capping of the polyether diamine followed by competitive reaction of the remaining isocyanate groups, either in trimerization reactions to form isocyanurate, or with the aromatic diamine chain extender to form ureas. The relative rates of reaction are determined by the chemical structures of the diamine, the concentration of the trimerization catalyst and the temperature. The parent d2/m/1.6 material comprises 33% by weight of polyether, whereas the two materials containing aromatic polyurea hard segments (d2/20d/1.6 and d2/20m/1.6) comprise 28% by weight of polyether.

The TEM micrographs of the d2/20d/1.6 and d2/m/1.6 copolymers (see *Figures 5a* and *b*, respectively) show real-space images similar to those in *Figure 2*. (In fact, comparison of *Figures 2b* and *5b* shows the effect of doubling the concentration of trimerization catalyst, namely a slight increase in the domain spacing, but a decrease in contrast.) According to the TEM results, the material containing DETDA, i.e. d2/20d/1.6, has a poor contrast structure with a smaller size-scale than material d2/m/1.6. These qualitative observations are in good agreement with the SAXS data shown in *Figure 6*, where the $(l\text{-}d)$ spacings obtained from the Lorentz-corrected scattering curves are, respectively, 74 Å and 114 Å for the material with DETDA (d2/20d/1.6), and without DETDA (d2/m/1.6); the corresponding, relative invariant values are 180 and 214, respectively. The addition of DETDA to the formulation prevents full development of the electron-density difference and reduces the observed domain spacing. The aromatic urea (which has a high $T_g$[8,9]) must coexist with both the polyether and the polyisocyanurate; it is possible that the addition of polyurea causes vitrification to occur at an earlier stage of structure development (i.e. smaller sizes and lower $Q'$ values).

The two TEM micrographs of the d2/20m/1.6 material (*Figures 5c* and *d*) show a different morphology to those discussed above. The lower-magnification micrograph features a random array of spherical inclusions, with a mean diameter of 1.5 $\mu$m, which is beyond the resolution of the SAXS experiment. These inclusions account for $\sim 20\%$ of the total volume, and are obviously neither pure polyisocyanurate, nor pure polyurea. The higher-magnification micrograph shows these inclusions to be superimposed on a background pattern similar to the real-space images in *Figures 2*, *5a* and *5b*. Furthermore, the inclusions have an internal structure with the same length-scale as the background pattern. These observations are supported by the SAXS data in *Figure 6* where copolymer d2/20m/1.6 has $(l\text{-}d)$ and $Q'$ values comparable to the parent d2/m/1.6 material. The matrix in d2/20m/1.6 must therefore have the same composition (in terms of electron-density modulation) as d2/m/1.6 and the extra aromatic glass must be contained in the inclusions. The upturn in $I'\mathbf{q}^2$ at low $\mathbf{q}$ for d2/20m/1.6 is most likely due to particle scattering from these inclusions.

The mechanism leading to the formation of inclusions has not been observed directly but is a result of competition between polymerization kinetics, chemical gelation and (micro)phase separation. Specifically, MDIPA reacts with diisocyanate at a rate comparable

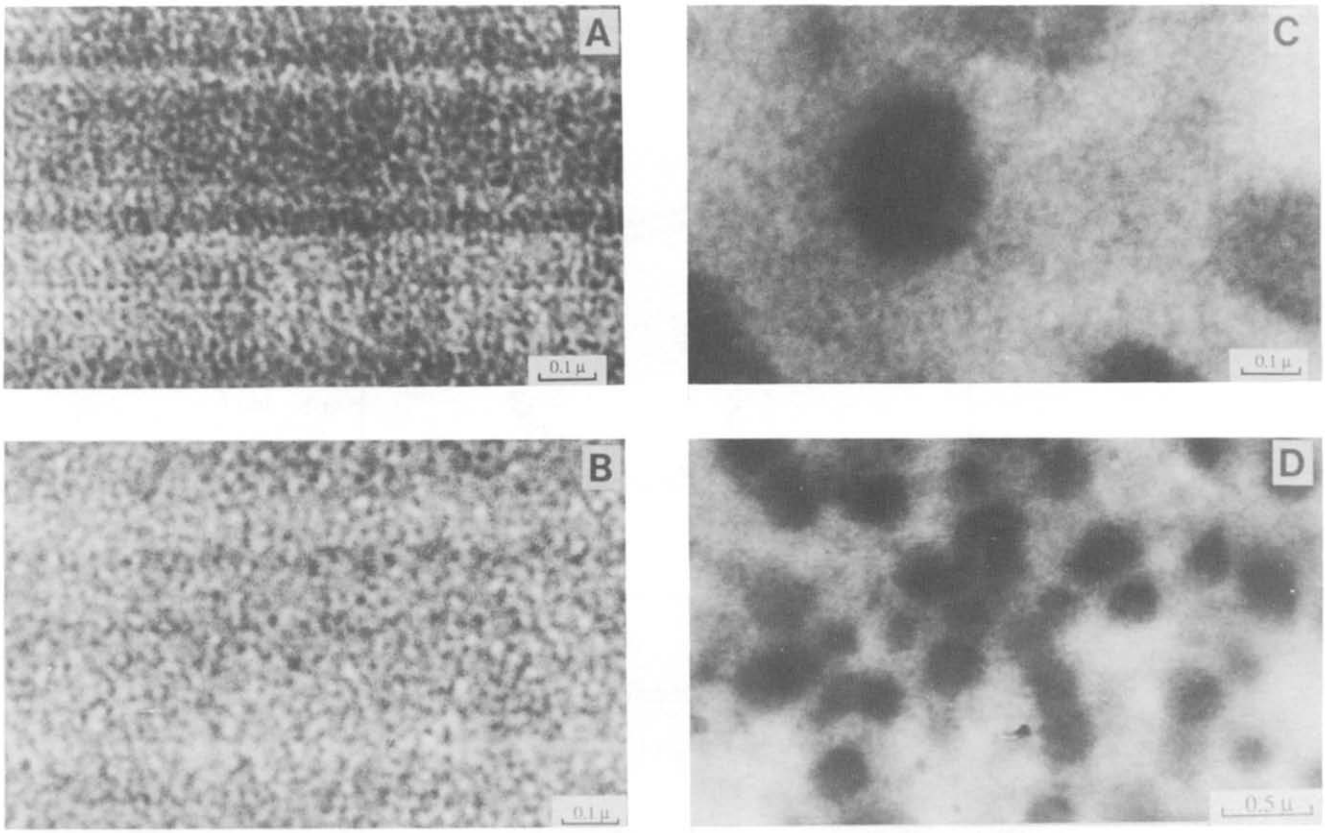


**Figure 5** TEM micrographs of the copolymers: d2/20d/1.6 (A); d2/m/1.6 (B); and d2/20m/1.6 (C) and (D)

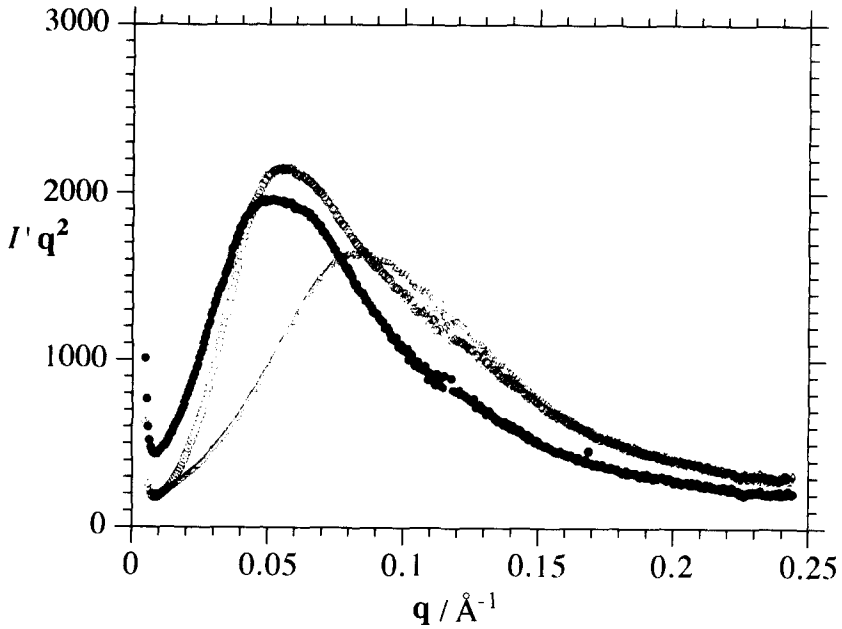


**Figure 6** Lorentz-corrected SAXS patterns for the copolymers: d2/20d/1.6 (△); d2/m/1.6 (○); and d2/20m/1.6 (●)

to the trimerization of the diisocyanate, although chemical gelation (at isocyanate conversions of ~60%) must occur after the onset of microphase separation ($l$-$d \sim 100$ Å). Unreacted MDI and MDIPA undergo microsyneresis (squeezing) from the lightly crosslinked block copolymer and then polymerize to form the inclusions of the crosslinked isocyanurate–urea. The narrow size distribution of the inclusions is a feature of heterogeneous nucleation and growth, with the nucleation event being microphase separation and gelation. In contrast, with d2/20d/1.6, DETDA reacts faster than MDIPA[1,9] and is incorporated in the trimerizing material. The gel point is delayed and little low-molecular-weight material remains to diffuse during post-gel microsyneresis. Consequently, the material shows only the microphase-separated morphology, without large inclusions.

The dynamic mechanical spectra shown in *Figure 7*

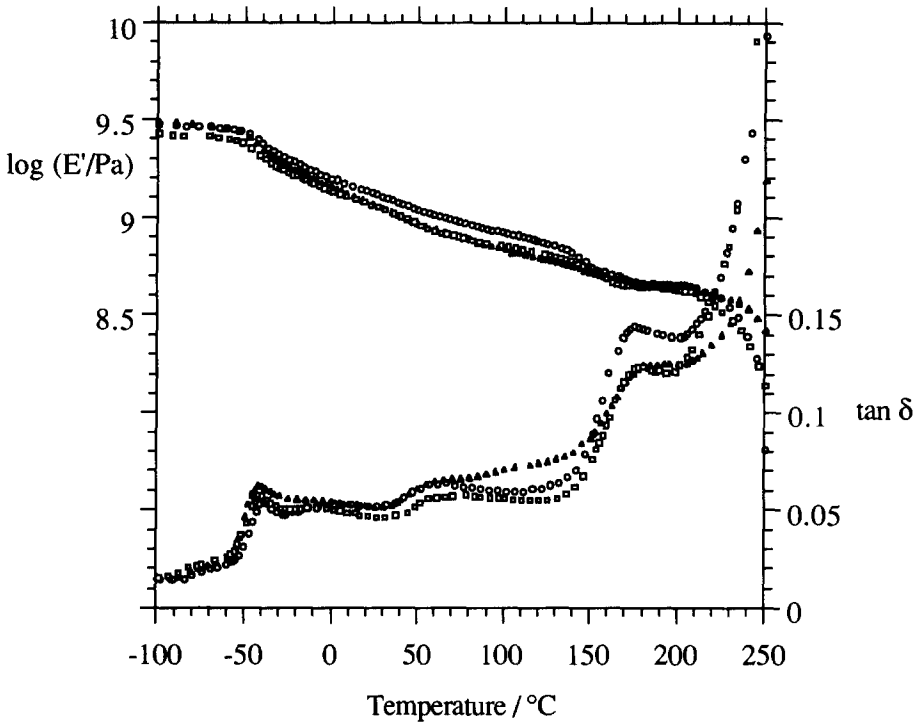


**Figure 7** D.m.t.a. curves for the copolymers: d2/20d/1.6(○); d2/m/1.6(△); and d2/20m/1.6(□)

illustrate the effects on modulus and damping of both chemical structure and morphology. In each case, the polyether glass transition is observed as a peak in tan $\delta$ and a drop in modulus at $\sim -30°C$. The isocyanurate glass transition is also observed as a peak in tan $\delta$ and a drop in modulus (followed by a rubbery plateau) at the higher temperature of $\sim 175°C$. The observation of two glass transition points confirms the existence of a microphase-separated morphology. The effects of morphology may be observed in the modulus–temperature behaviour. Both of the d2/20d/1.6 and d2/m/1.6 materials appear to have co-continuous morphologies from TEM observations. However, the d2/20d/1.6 material has a higher volume fraction of organic glass, and it therefore has a higher modulus than the d2/m/1.6 material over the entire temperature range. The d2/20d/1.6 and d2/20m/1.6 materials have the same volume fractions of organic glass, although the latter has a discontinuous structure with glassy inclusions, and consequently has a lower modulus above the polyether glass transition point. The tensile stress–strain data in *Table 2* confirm the relationship between modulus (as determined by d.m.t.a.) and morphology. The weak feature in tan $\delta$ and corresponding changes in slope of $E'$ observed at $\sim 50°C$ for all three materials, are similar to those discussed previously for the as-moulded d2/m/0.6 material. This behaviour is an indication of phase mixing[8,9,16,25].

Comparison of the d.m.t.a. and SAXS data for the d2/m/1.6 and d2/m/0.6/150 materials shows the former to have a poorer microphase separation, as evidenced by the lower $Q'$ value and the existence of the phase-mixed tan $\delta$ peak, despite the phase-mixed material having a bigger (*1-d*) spacing.

*Effects of soft segment structure*

The two TEM micrographs of t5/m/1.6 in *Figures 8a* and *b* show a morphology similar to that discussed above for d2/20m/1.6. The lower-magnification micrograph

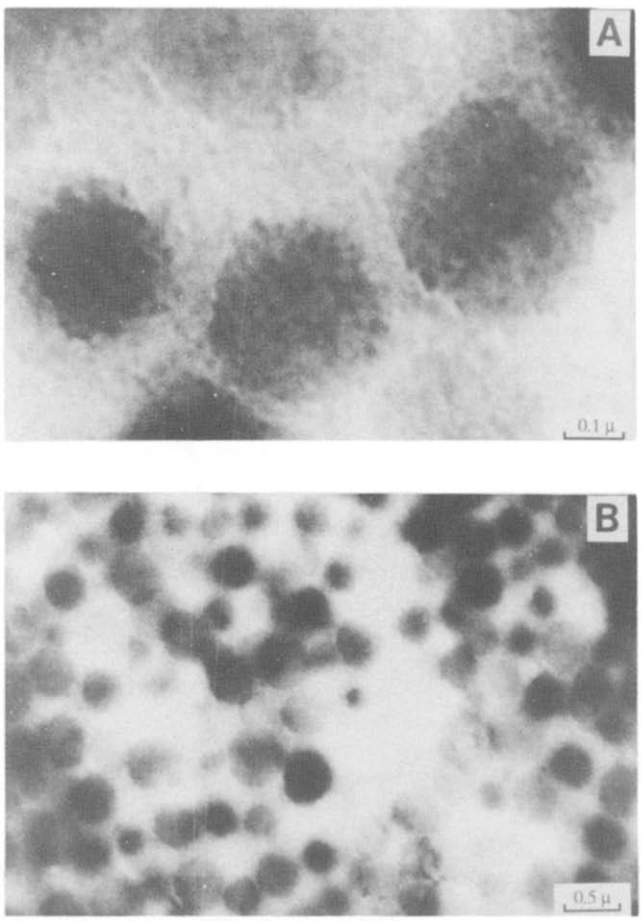


**Figure 8** TEM micrographs of the copolymer t5/m/1.6, at different magnifications

features a random array of spherical inclusions with a mean diameter of 1.9 $\mu$m, accounting for $\sim 25\%$ of the volume. The higher-magnification micrograph shows these inclusions to be superimposed on a background

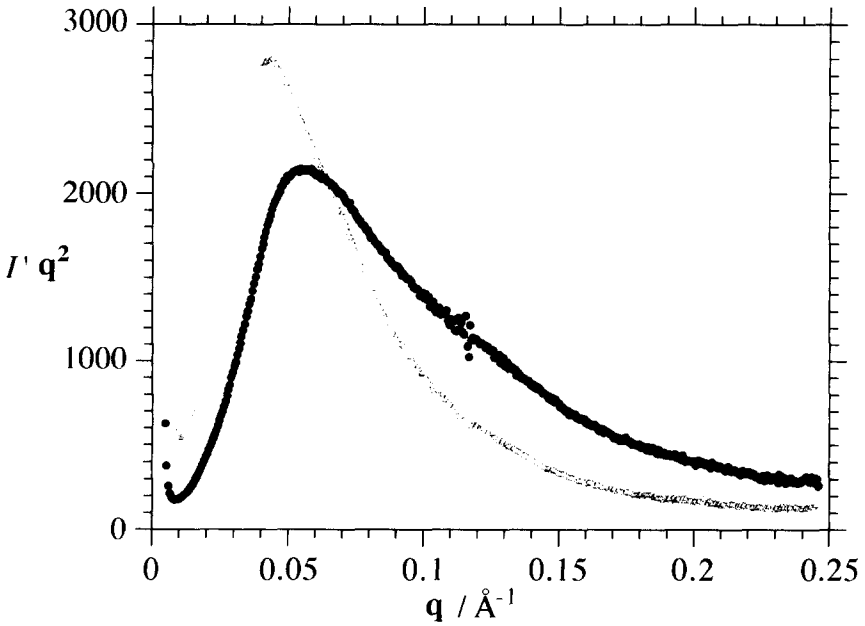


**Figure 9** Lorentz-corrected SAXS patterns for the copolymers: d2/m/1.6 (●) and t5/m/1.6 (△)

pattern, similar to the real-space images in *Figures 2*, *5a* and *5b*, with a characteristic length of ~150 Å. Furthermore, the inclusions have an internal structure with the same length-scale as the background pattern. These observations should be compared with those made for d2/m/1.6, whose micrograph forms *Figure 5b*, noting that the only difference between the d2/m/1.6 and t5/m/1.6 materials is in the replacement of the 2000-molecular-weight diamine with a 5000-molecular-weight triamine. The increase in the characteristic size in the morphology is expected, since the radius of gyration, $R_g$, of T5000 is ~1.8 times greater than that of D2000. However, the existence of spherical inclusions, of what must be isocyanurate-rich material, is unexpected.

SAXS data for t5/m/1.6 and the homologous d2/m/1.6 material are presented in *Figure 9*; the (*1-d*) spacings of 153 and 112 Å, respectively, are in good agreement with TEM. The relationship between $R_g$ and the degree of polymerization, $N$, according to De Gennes[26] is $R_g \sim N^{1/2}$. Furthermore, for strongly segregated block copolymers, Helfand and Wasserman[27] have shown the observed domain spacing to be directly related to $R_g$, i.e. $(1\text{-}d) \sim R_g \sim N^{2/3}$. Assuming the RIM copoly(isocyanurate–urea)s to be strongly segregated block copolymers, then a 1.8 increase in the radius of gyration should lead to a change of equal magnitude in the observed (*1-d*) spacing. The similarity in the values of $Q'$ indicate that the matrix in the t5/m/1.6 material has essentially the same composition (in terms of electron density) as d2/m/1.6, since the relative invariant measures only the square of the electron-density difference. The inclusions must contain aromatic glass, so that the volume fraction of glassy material in the lamellar matrix is reduced. Thus from geometric considerations the observed value of (*1-d*) is reduced, when compared with that predicted for the well segregated block copolymer. The upturn in $I'\mathbf{q}^2$ at low $\mathbf{q}$, for t5/m/1.6, is again most likely due to particle scattering from these inclusions.

The effects of morphological differences on dynamic mechanical behaviour are illustrated in *Figure 10* for the d2/m/1.6 and t5/m/1.6 copolymers. Replacing D2000 by T5000 results in a more intense polyether glass transition at ~ −30°C. For both materials, the isocyanurate glass transition is observed as a shoulder on a rising $\tan\delta$ curve and a drop in modulus (followed by a rubbery plateau) at ~175°C. The large difference in the modulus–temperature behaviour above the polyether glass transition is due to morphology. The t5/m/1.6 material has the same volume fraction of organic glass as d2/m/1.6, but shows a lower value of modulus over the entire temperature range. Both materials appear to have a co-continuous morphology from TEM studies, except that in t5/m/1.6 there is also a discontinuous structure of glassy inclusions. The tensile stress–strain data shown in *Table 2* confirm this behaviour. Furthermore, t5/m/1.6 also has the weak peak in $\tan\delta$ and a corresponding change in the slope of $E'$ at ~50°C, which is associated with the breakdown of hydrogen bonding between the ether oxygens and urea carbonyls; these features are an indication of phase mixing.

The incorporation of a chain extender into the t5-systems results in similar changes in the morphology and mechanical properties as discussed above for the d2-systems. Thus, the data in *Table 2* for t5/20d/1.6 (compared to t5/m/1.6), and the data for d2/20d/1.6 (compared to d2/m/1.6), show that the addition of a DETDA-based hard segment leaves the morphology qualitatively unchanged, but with reductions in $L$, (*1-d*), and $Q'$. Furthermore, addition of DETDA results in higher values of the modulus, strength and ultimate elongation. The different morphologies of the d2- and t5-systems are, therefore, related solely to the molecular architecture (linear *versus* branched) of the polyether oligomers and indicate that structure develops during the initial stages of polymerization since the amines react almost instantaneously and their reaction products dominate the subsequent thermodynamic processes occurring during solidification. Impingement mixing of amine-functionalized polyether oligomers with MDI does not always lead to the formation of a perfect mixture, as shown by Willkomm[25]. The most probable distribution could only be achieved by using very high Reynolds

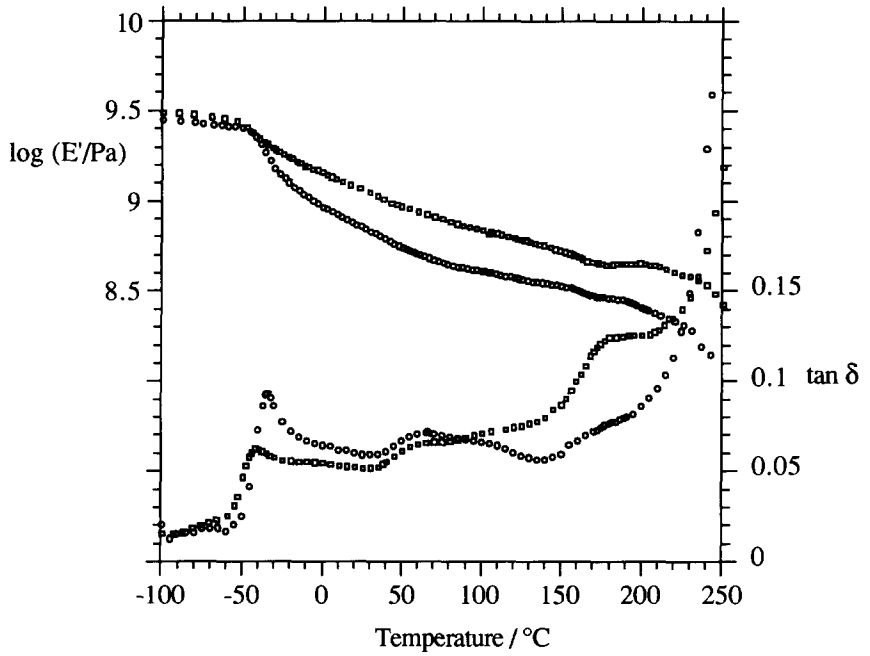


**Figure 10** D.m.t.a. curves for the copolymers: d2/m/1.6 (□) and t5/m/1.6 (○)

numbers (>800) for mixtures of polyether diamines and MDI at a stoichiometric ratio, $r=10$. When T5000 is mixed with MDI (at $r=10$), an inhomogeneous 'stringy' solid was extruded from the mixhead, irrespective of Reynolds number. This stringy structure corresponds to the initial striations formed during the impingement mixing process. Chemical gelation occurred in milliseconds, a time-scale which is equivalent to the residence time of the materials in the mixhead. Theoretically[28], chemical gelation occurs only in the stoichiometry interval, $f-1 \geqslant r \geqslant 1/f-1$, for $RA_2+RB_f$ polymerizations. That chemical gelation occurs in the reaction between a diisocyanate and a triamine ($f=3$) indicates that a local stoichiometry of $r \leqslant 2$ exists in the striations. The loosely crosslinked system sets the initial (block copolymer) morphology with ($1$-$d$)=150 Å at very low (<20%) conversions of isocyanate groups, and starts to exclude the unreacted diisocyanate from the gel by microsyneresis (squeezing). A heterogeneous nucleation and growth process accounts for the nearly monodisperse size distribution of the inclusions, which are subsequently crosslinked.

## SUMMARY AND CONCLUSIONS

A series of novel RIM copoly(isocyanurate–urea)s have been formed by reacting a polyisocyanate and a polyether polyamine (with an aromatic diamine chain extender) in the presence of an organic catalyst. A polyether diamine (D2000) and a polyether triamine (T5000) were used to study the effects of functionality on the morphology and properties of copoly(isocyanurate–urea)s. An aromatic diamine chain extender, either DETDA or MDIPA, was also used in some systems to modify the glassy isocyanurate structure, resulting in the formation of tougher materials. Properties of RIM materials were shown to be dependent on their non-equilibrium morphology which resulted from competition between polymerization kinetics, chemical gelation and (micro)phase separation. D.m.t.a. confirmed the existence of a microphase-separated morphology, the scale of which was determined by SAXS and TEM. The SAXS data were analysed in the framework of a lamella system, despite the TEM micrographs being somewhat inconclusive. The degree of segmental mixing, inferred from the d.m.t.a. modulus–temperature dependence between the polyether (~ −50°C) and isocyanurate (~170°C) glass transition temperatures, was in good agreement with that measured by the invariant $Q'$ from SAXS. The rate of the isocyanate trimerization reaction and the rate between the chain extender and isocyanate in the D2000/DETDA system were similar and the high-modulus (~1.5 GPa) materials thus formed were shown by SAXS and TEM to have an isotropic, co-continuous morphology ($1$-$d$~100 Å). Replacing D2000 with T5000 resulted in materials with heterogeneous morphologies, irrespective of variations in composition or processing conditions. Materials, which were shown by TEM to contain isolated glassy particles (~1 μm in size), were formed when chemical gelation occurs at low isocyanate conversions (50–60%) and had lower moduli (~0.7 GPa) than those with the isotropic morphology. In systems based on D2000 and MDIPA the chain extender–isocyanate reaction was slower than the trimerization reaction and this also resulted in the formation of isolated glassy particles. The results of these studies have therefore established correlations between processing, morphology and the dynamic mechanical thermal and tensile stress–strain properties for a systematic series of copoly(isocyanurate–urea)s.

## ACKNOWLEDGEMENTS

The support of the SERC (with minor grant BAP 19/36) is gratefully acknowledged. The authors also thank Wim Bras of the SERC Daresbury Laboratory for technical assistance and Arthur Wilkinson for valuable suggestions during this research. Original support for the development of these materials (see ref. 14) was kindly provided by Kobe Steel Europe Limited.

## REFERENCES


1 Macosko, C. W. 'Fundamentals of Reaction Injection Moulding', Hanser, Munich, 1989
2 Carleton, P. S., Waszeciak, D. P. and Alberino, L. M. *J. Cell. Plast.* 1985, **21**, 409
3 Vespoli, N. P. and Alberino, L. M. *Polym. Processing Eng.* 1985, **3**, 127
4 Klempner, D., Frisch, K. C. and Wang, C. L. *Adv. Urethane Sci. Technol.* 1984, **9**, 102
5 Nelson, D. *Plast. Eng.* 1987, 29
6 Wang, C. L., Klempner, D. and Frisch, K. C. *J. Appl. Polym. Sci.* 1985, **30**, 4337
7 Carleton, P. S., Ewen, J. H. and Raymore, H. E. US Patent 4 126 741, 1978; 4 126 742, 1978
8 Ryan, A. J., Still, R. H. and Stanford, J. L. *Plast. Rubber Processing Appl.* 1990, **13**, 99
9 Ryan, A. J. and Stanford, J. L. in 'Comprehensive Polymer Science', Vol. 5 (Eds G. Allen and J. C. Bevington), Pergamon, Oxford, 1988, Ch. 23, p. 427
10 Dominguez, R. J. G. *J. Cell. Plast.* 1984, **20**, 433
11 Macosko, C. W. 'Fundamentals of Reaction Injection Moulding', Hanser, Munich, 1989, Ch. 2, p. 11
12 Gibson, P. E., Vallance, M. A. and Cooper, S. L. in 'Developments in Block Copolymers', Vol. 1 (Ed. I. Goodman), Applied Science, London, 1982, p. 217
13 Abouzahr, S. and Wilkes, G. L. in 'Processing, Structure and Properties of Block Copolymers', (Ed. M. J. Folkes) Elsevier, New York, 1985, p. 165
14 Ryan, A. J., Stanford, J. L. and Wilkinson, A. N. (Kobe Steel Europe Limited) Br. Pat. Appl. GB 90/21 917.1, 1990
15 Stagg, H. E. *Analyst (London)* 1946, **71**, 557
16 Wilkinson, A. N., PhD Thesis, Victoria University of Manchester, 1990
17 Ryan, A. J., Macosko, C. W. and Bras, W. *Macromolecules* 1992, **25**, 6277; Lewis, R. A., Sumner, I., Berry, A., Bordas, J., Gabriel, A., Mant, G. R., Parker, B., Roberts, K. and Worgan, J. *Nucl. Instrum. Methods* 1988, **A273**, 773
18 Baltá-Calleja, F. J. and Vonk, C. G. 'X-Ray Scattering of Synthetic Polymers', Elsevier, Amsterdam, 1989
19 Porod, G. *Kolloid-Z. Z. Polym.* 1951, **124**, 83; 1952, **125**, 51; 1952, **125**, 108
20 Pannone, M. C. and Macosko, C. W. *Polym. Eng. Sci.* 1988, **28**, 660
21 Cahn, J. W. and Hilliard, J. E. *J. Chem. Phys.* 1958, **28**, 258
22 Chen-Tsai, C. H. Y., Thomas, E. L., MacKnight, W. J. and Schneider, N. S. *Polymer* 1986, **27**, 659
23 Ryan, A. J. *Polymer* 1990, **31**, 707
24 Olabisi, O., Robeson, L. M. and Shaw, M. T. 'Polymer–Polymer Miscibility', Academic, New York, 1979
25 Willkomm, W. R., PhD Thesis, University of Minnesota, 1990
26 De Gennes, P. G. 'Scaling Concepts in Polymer Physics', Cornell University Press, Ithaca, 1979
27 Helfand, E. and Waserman, Z. R. in 'Developments in Block Copolymers', Vol. 1 (Ed. I. Goodman), Applied Science, London, 1982, p. 99
28 Flory, P. J. 'Principles of Polymer Chemistry', Cornell University Press, Ithaca, 1953